# Synthesis of *s*-Triazine-Based Hyperbranched Polyurethane for Novel Carbon-Nanotube-Dispersed Nanocomposites

**Sibdas Singha Mahapatra, Sravendra Rana, Jae Whan Cho**

*Department of Textile Engineering, Konkuk University, Seoul 143-701, Korea*

Received 5 January 2010; accepted 12 August 2010
DOI 10.1002/app.33155
Published online 19 October 2010 in Wiley Online Library (wileyonlinelibrary.com).

**ABSTRACT:** *s*-Triazine-based hyperbranched polyurethanes (HBPUs) with different hard segments were synthesized by $A_2 + B_3$ approach. Various kinds of multiwalled carbon nanotube (MWNT) nanocomposites with HBPU were prepared to investigate an impact of hyperbranched polymer on dispersion of MWNTs in the polymer matrix and the resulting properties of nanocomposites. Synthesized HBPUs were characterized using FTIR and NMR measurements. The highly branched structures were found very effective in enhancing the pristine MWNT dispersion in the polymer matrix. As a result, the MWNT-reinforced HBPU nanocomposites showed a steep increase in the yield stress and modulus and enhanced shape memory effect with an increase of hard segment and MWNT loading. © 2010 Wiley Periodicals, Inc. J Appl Polym Sci 120: 474–483, 2011

**Key words:** nanocomposites; hyperbranched; polyurethanes; dispersions; mechanical properties

## INTRODUCTION

Carbon nanotubes (CNTs) can be used as an ideal reinforcing agent for polymer composites[1,2] because of their excellent mechanical, electrical, thermal, and magnetic properties.[3,4] However, despite significant research progress, successful applications of such composite systems require well-dispersed nanotubes with the host matrix and good solubility in organic solvents, which unfortunately is not satisfactorily realized. Processing of CNT–polymer nanocomposites such as film formation, fiber spinning, and electrospinning is not easy because of the poor solubility and strong intermolecular interaction of CNTs.[5] Thus, many research groups have focused on functionalizing CNTs with various organic and organometallic structures and linear polymers to increase their solubility.[6,7] CNT functionalization, including acid treatment of CNTs, is usually used to achieve better CNT dispersion, but it damages the CNT surface and disrupts the structural integration of CNTs.[8]

As an alternative approach, hyperbranched polymer may be used to improve the dispersion of CNTs into the polymer matrix.[9–11] The controlled macromolecular architecture of hyperbranched polymers has been recognized as an important tool to obtain polymers with tailored properties. For example, highly branched polymers generally exhibit good solubility; lower melt and solution viscosity; presence of empty, internal cavities; and extremely high density of functional groups at the surface.[12–15] Therefore, it may increase the solubility of CNTs and enable their applications. Further, hyperbranched polymers can be prepared by single-step process and thus obtained in a large scale at reasonable cost, making them more interesting for commercial applications.

On the other hand, polyurethanes (PUs) have gained tremendous importance because of their various applications as thermoplastic elastomers, foams, fibers, adhesives, coating materials, and so forth.[16,17] Recently, it has also attracted great interest as shape memory polymer compared to shape memory alloys because of their low cost, good processing ability, high shape recoverability, and wide range of shape recovery temperature.[18,19] For high performance applications of PU, researchers have improved its thermal, electrical, and mechanical properties by adding nanofillers into the polymer matrix.[20–22] Also, the design of PU with heterocyclic moiety like *s*-triazine unit in the structure has profound effects on the physicochemical and thermal properties and its processability.[23–25] Three-dimensional (3D) heterocyclic structure would be more suitable to afford the pathway for well-dispersed CNT nanocomposites. To the best of our knowledge, there are few examples of solubilization of CNTs using physical adsorption of hyperbranched polymer,[26,27] but there is no report on preparation of hyperbranched

*Correspondence to:* J. Whan Cho (jwcho@konkuk.ac.kr).
Contract grant sponsor: Korea Research Foundation; contract grant number: KRF-2006-005-J03302.

**TABLE I**
**Compositions and Compounding Formulations of Samples**

| Sample codes | Feed weight (g) | | | | MWNT (wt %) | Hard segment content (wt %) |
|---|---|---|---|---|---|---|
| | MDI | PCL | BD | TAPT | | |
| HBPU 30 | 1.0 | 4.0 | 0.135 | 0.60 | – | 30 |
| HBPU 37 | 1.0 | 3.0 | 0.145 | 0.60 | – | 37 |
| HBPU 42 | 1.0 | 2.5 | 0.200 | 0.60 | – | 42 |
| HBNT 0.3 | 1.0 | 3.0 | 0.145 | 0.60 | 0.3 | 37 |
| HBNT 1.5 | 1.0 | 3.0 | 0.145 | 0.60 | 1.5 | 37 |
| HBNT 3.0 | 1.0 | 3.0 | 0.145 | 0.60 | 3.0 | 37 |

shape memory PU with *s*-triazine ring and their CNT-based nanocomposites.

In this study, the *s*-triazine-based hyperbranched PUs (HBPUs) were synthesized and used to prepare nanocomposites with novel dispersion of pristine multiwalled carbon nanotubes (MWNTs). The structural, thermal, mechanical, and shape memory properties and dispersion of MWNTs for the nanocomposites were investigated.

## EXPERIMENTAL

### Materials

Poly(ε-caprolactone)diol (PCL) with a molecular weight of 3000 g/mol was received from Solvay, Co., Warrington, UK, and 1,4-butanediol (BD) was obtained from Junsei Chemical, Tokyo, Japan. 4,4′-Methylenebis(phenylisocyanate) (MDI), 4-aminophenol, and 2,4,6-trichloro-[1,3,5]triazine were purchased from Aldrich, St. Louis, MO, USA. MWNTs with diameter, length, and purity of about 10–20 nm, 20 μm, and 95%, respectively, were purchased from Iljin Nanotech, Seoul, Korea. *N*,*N*′-dimethylformamide (DMF) was used after purification by the conventional technique and stored with 4 Å type molecular sieves.

### Synthesis of 2,4,6-tri(4′-aminophenol)-1,3,5-triazine

In a two-neck, round-bottom flask, 3.00 g (16.26 mmol) of 2,4,6-trichloro-[1,3,5]triazine was stirred and dissolved in 100 mL acetone. Potassium carbonate (3.38 g; 24.4 mmol) was added to it, which was cooled to 0°C. After forming the slurry, 5.328 g (48.78 mmol) of 4-aminophenol was added portionwise. The suspension mixture was slowly warmed to room temperature and then heated under reflux for 36 h. The solid obtained was filtered and further purified. Yield = 86%; $^1$H NMR (DMSO-$d_6$, δ, ppm): 9.03 (OH), 8.71 (NH), 6.65–7.46 (Ph-H); FTIR: 3380, 3253, 1620, 1519, 1490 cm$^{-1}$.

### Synthesis of HBPU

*s*-Triazine-based HBPU with different hard segments was synthesized by two-step procedure as follows. In a 500-mL four-neck cylindrical vessel equipped with a mechanical stirrer and nitrogen inlet, first the prepolymer was prepared from the reaction of required amount of MDI and PCL in dry DMF. The reaction was continued at 70°C for 3 h. After the completion of prepolymer synthesis, the system was cooled to 0°C and required amounts of 2,4,6-tri(4′-aminophenol)-1,3,5-triazine (TAPT) and BD solution in DMF were added into it. The reaction temperature was then increased slowly up to 110°C and the reaction was continued for 3 h under the same condition. After the completion of reaction, the final product solution was dried in hot air oven at 50°C to obtain the polymer films. HBPU of different compositions was synthesized by changing the weight ratio of monomers (Table I), such as hard segment 30, 37, and 42% and coded as HBPU 30, HBPU 37, and HBPU 42, respectively. The synthesis of the model compounds of TAPT with one, two, and three equivalents of phenyl isocyanate was performed separately, exactly in the same way as described in the second stage of the hyperbranched polymer synthesis.

### Preparation of MWNT nanocomposites

The HBPU 37/MWNT nanocomposite films were prepared by solvent casting using different weight compositions (0.3, 1.5, and 3.0 wt %) of MWNTs with respect to HBPU 37. Before this, the required amount of MWNTs was sonicated in DMF separately by high-power horn-type sonicator for 1 h. The DMF solution of MWNTs was mixed into a PU solution and stirred on a magnetic stirrer for 24 h at room temperature. The final composite solution at 15 wt % concentration in DMF was poured on a glass petri dish, and the solvent was evaporated at 50°C in hot air oven to obtain the polymer films. The samples were coded (Table I) as HBNT 0.3, HBNT 1.5, and HBNT 3.0 for the HBPU 37/MWNT nanocomposites, where the number in the code

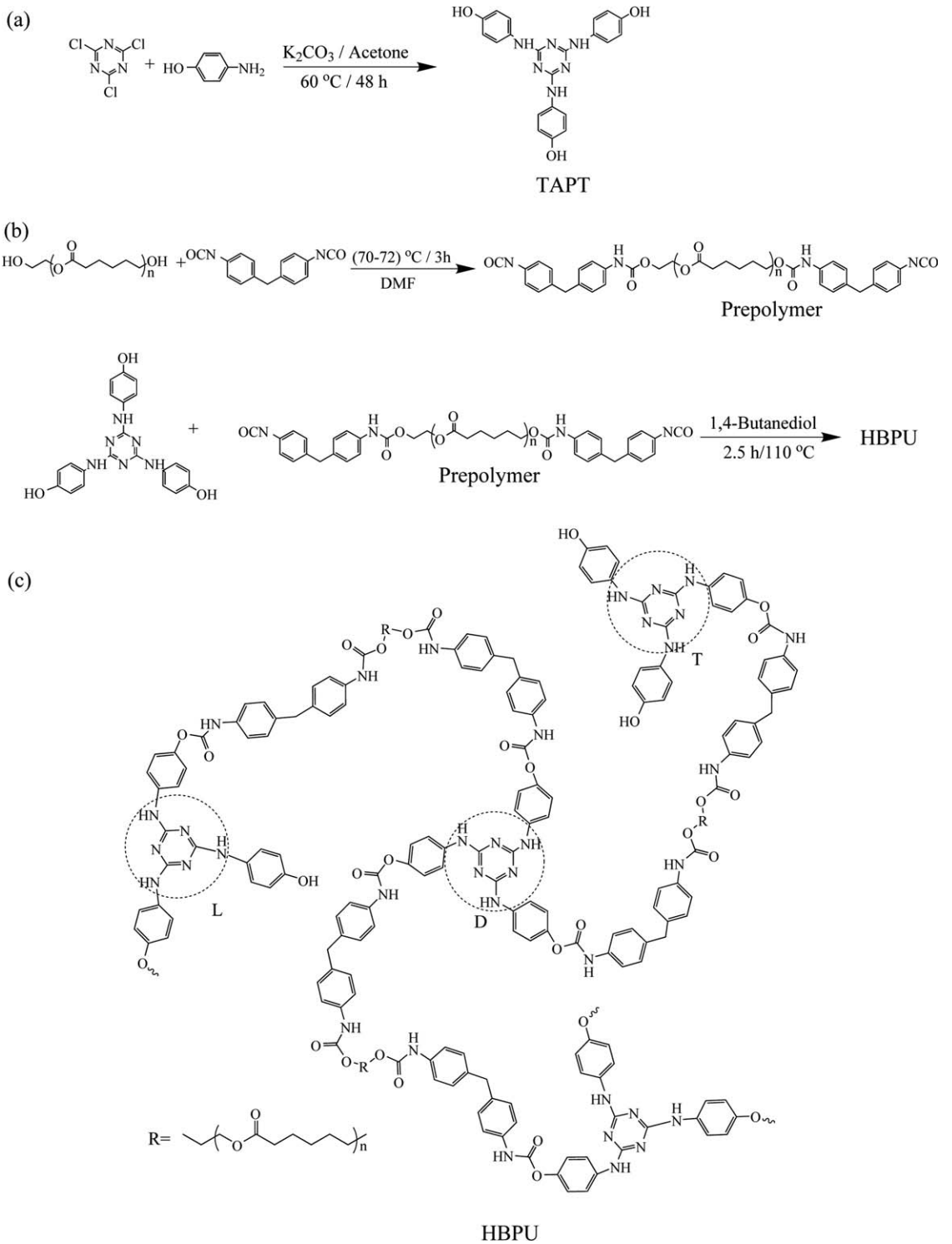


**Scheme 1** Synthesis of TAPT monomer (a) and HBPU (b); (c) schematic diagram of hyperbranched polymer.

indicates the MWNT content in wt % with respect to the polymer matrix (HBPU 37).

## Characterization

FTIR spectra for the compounds were recorded in a Jasco FT-IR 300E (Tokyo, Japan) with an attenuated total reflectance method and by using KBr pellets for film and powder samples, respectively. $^1$H NMR spectra of the samples were recorded with Bruker 600-MHz NMR spectrometer by using *N*,*N*′-dimethylsulphoxide-$d_6$ (DMSO-$d_6$) as the solvent and tetramethylsilane (TMS) as the internal standard. The molecular weight of hyperbranched polymers was determined by gel permeation chromatography (GPC) analysis (Model 515; Water, Milford, USA) using

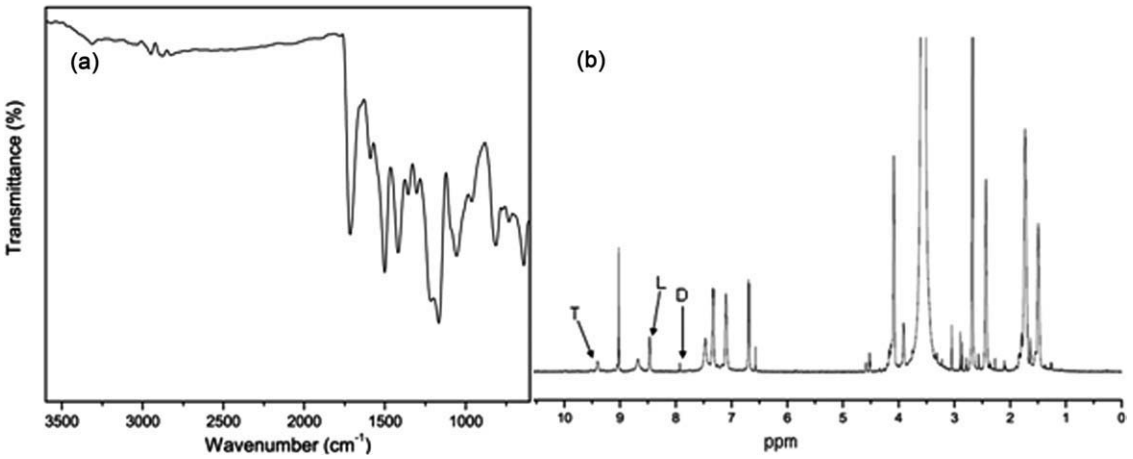


**Figure 1** FTIR (a) and $^1$H NMR (b) spectra of HBPU 37.

DMSO as the solvent. Differential scanning calorimetry (DSC) measurements were carried out using TA instrument 2010 (Du Pont, New Castle, DE) thermal analyzer in a temperature range of −50 to 250°C, at a heating rate of 10°C/min in liquid nitrogen. Thermogravimetric (TG) analyses (TGA) were carried out in TA Q50 thermal analyzers, using the nitrogen flow rate of 30 mL/min and at the heating rate of 10°C/min. X-ray diffraction was performed using Rigaku Rint 2100 series (Tokyo, Japan) X-ray diffractometer with Cu Kα radiation at a scan rate of 5°/min. The MWNT dispersion in the nanocomposites was analyzed on the basis of its surface morphology using a field emission scanning electron microscope (FE-SEM; S-4300SE, Hitachi, Tokyo, Japan), using transmission electron microscopy (TEM; JEM 2100F, JEOL, Tokyo, Japan) and atomic force microscopy (AFM; XE100, PSIA, Suwon, Korea). SEM images were obtained from the cross sections of fractured samples in liquid nitrogen. For the measurements of AFM, the samples [0.001% (w/v) in DMF] were prepared by spin coating in 1000 rpm speed for 150 s on indium tin oxide (ITO) glass and measured in the contact mode. The mechanical properties of the samples were measured at room temperature using a tensile tester machine (Instron 4468) according to the ASTM D638 test method. The dimensions of the test specimens were $60 \times 2.9 \times T$ mm$^3$, where $T$ indicates a thickness that is variable. The gauge length and strain rate were 10 mm/min and 20 mm/min, respectively. In each case, at least five measurements were taken. The rheological studies of HBPU/MWNT composite were done with the help of CVO100, Malvern, Worcestershire, UK. All the experiments were performed at 180°C using a parallel plate of 20-mm diameter (PP20) with a gap size of 150 μm. The study was carried out at controlled stress of 10 Pa under the variation of frequency 1–100 s$^{-1}$. The shape-memory effect was checked by a tensile test with a UTM equipped with a temperature-controlled thermal cabinet. For measurement of the shape retention rate, a specimen with length $L_o$ was strained to 100% at 45°C and kept at that temperature for 2 min. The specimen under the strain was quenched at −30°C and left at that temperature for 30 min after removal of load; measurement of the deformed length $L_1$ followed. The specimen was again heated at 45°C, kept at that temperature for 5 min, quenched again at −30°C, and kept at this temperature for 30 min. From the final specimen length $L_2$, shape retention and shape recovery in percentage could be calculated using eqs. (1) and (2):

$$\text{Shape retention} = (L_1 - L_0)/L_0 \times 100 \quad (1)$$

$$\text{Shape recovery} = (2L_0 - L_2)/L_0 \times 100 \quad (2)$$

This whole procedure was repeated three times for the shape memory test of each sample.[28]

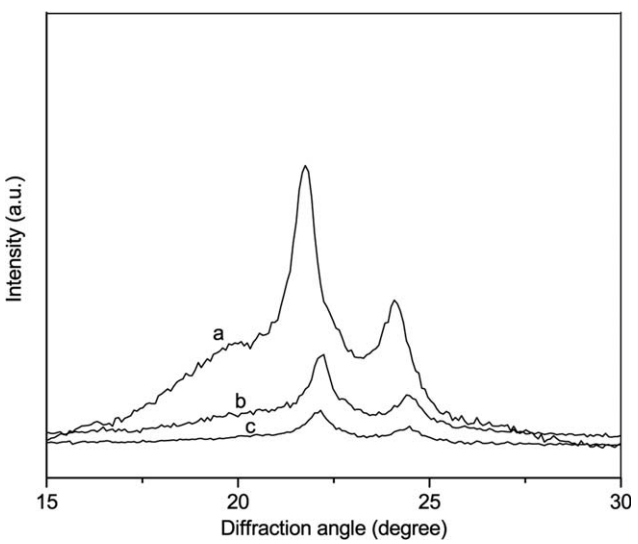


**Figure 2** X-ray diffractogram of HBPU 30 (a), HBPU 37 (b), and HBPU 42 (c).

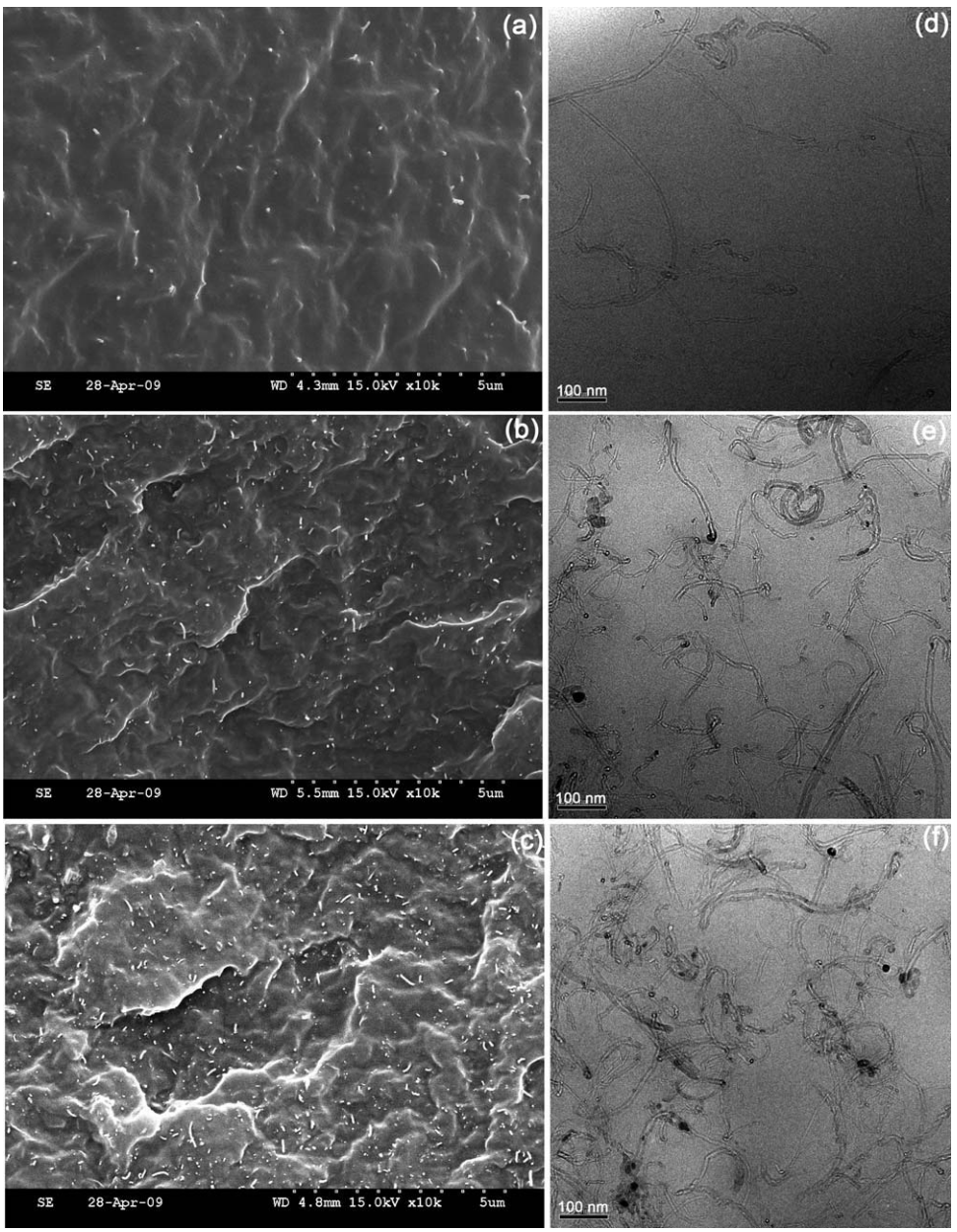


**Figure 3** SEM photographs of HBNT 0.3 (a), HBNT 1.5 (b), and HBNT 3.0 (c), and TEM images of HBNT 0.3 (d), HBNT 1.5 (e), and HBNT 3.0 (f).

## RESULTS AND DISCUSSION

### Synthesis and characterization of HBPU

The HBPUs have been synthesized by two-step process by using $A_2 + B_3$ approach with different hard segments. Here, PCL-based –NCO-terminated prepolymer or excess MDI as $A_2$ monomer and triazine-based 2,4,6-tri(4-aminophenol)-1,3,5-triazine (TAPT) as $B_3$ monomer were used to prepare the thermoplastic PU (Scheme 1). The addition of $B_3$ monomer at low temperature and high dilution was used to avoid the gel formation. Three different hyperbranched polymers with different hard segments but the same NCO/OH ratio (1 : 1) were synthesized by changing the compositions of the PCL, TAPT, BD, and MDI. The composition containing different hard segments is given in Table I.

The synthesized polymers are well characterized by FTIR and $^1$H NMR spectroscopy (Fig. 1). In FTIR spectra of HBPU 37 [Fig. 1(a)], the absorption band at about 2250–2270 and 3400 $cm^{-1}$ due to NCO and OH groups, respectively, disappeared, which confirmed the completion of the polymerization reaction.[29] It has also been seen that the appearance of a narrow bands at 3320 $cm^{-1}$ is due to presence of –NH stretching vibration. The absorption peaks at 1720 and 1610 $cm^{-1}$ correspond to –C=O in the ester and C=C stretching, respectively, and the IR peak at

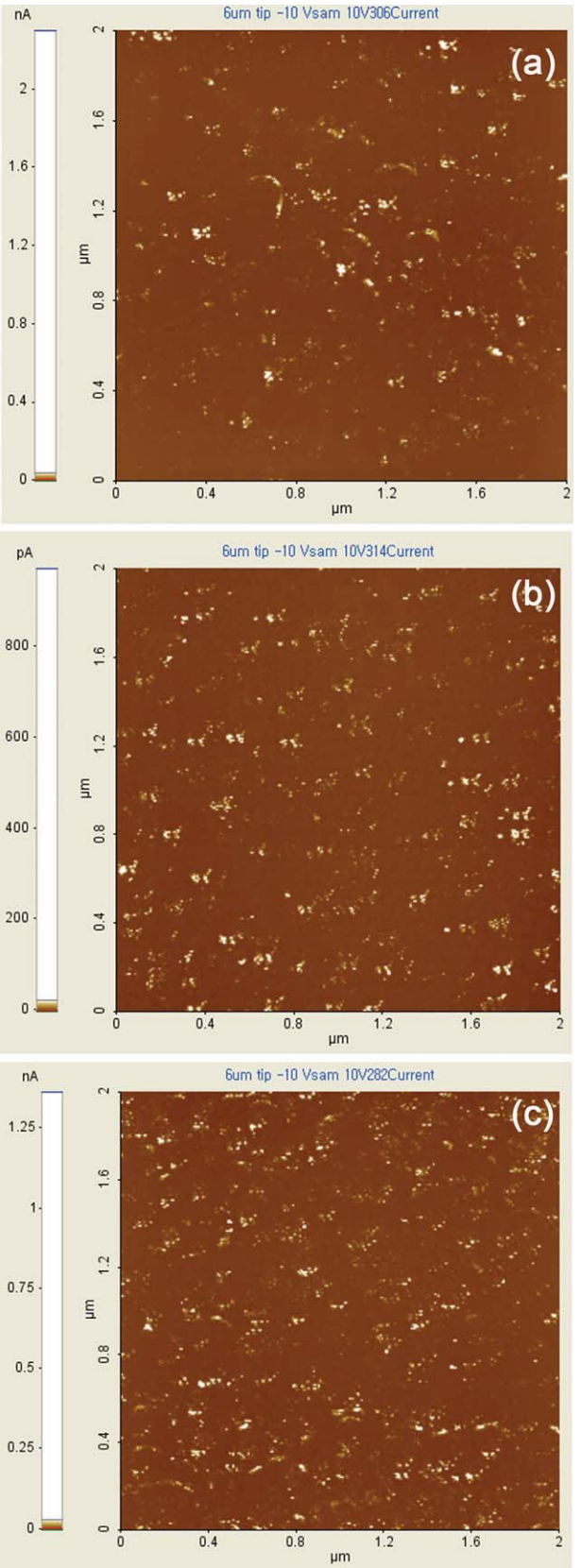


**Figure 4** AFM current images of HBNT 0.3 (a), HBNT 1.5 (b), and HBNT 3.0 (c) nanocomposites. [Color figure can be viewed in the online issue, which is available at wileyonlinelibrary.com.]

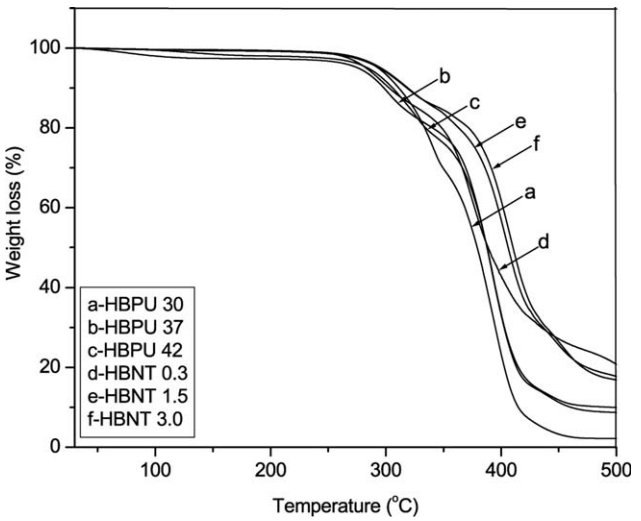


**Figure 5** TGA thermograms of pure HBPU and MWNT/HBPU nanocomposites.

1525 $cm^{-1}$ is due to –N–H bending. The structure of the PUs was further confirmed by $^1H$ NMR spectroscopy. The $^1H$ NMR spectra of the HBPU 37 [Fig. 1(b)] indicated the presence of important peaks for the different types of protons. Three different peaks at $\delta = 9.5$, 8.5, and 8.0 ppm appeared for the secondary –NH protons of the urethane linkages, and this confirms the presence of three different units: terminal (T), linear (L), and dendritic (D) units [Fig. 1(b)]. The terminal –OH and –NH attached with triazine unit appeared at $\delta = 9.1$ and 8.7 ppm, respectively. The aliphatic $CH_2$ protons appeared at $\delta = 4.4$–1.3 ppm. The protons for the aromatic moieties appeared at $\delta = 7.3$–6.6 ppm as a multiplet, perhaps because of the presence of different types of chemical environments as a large number of

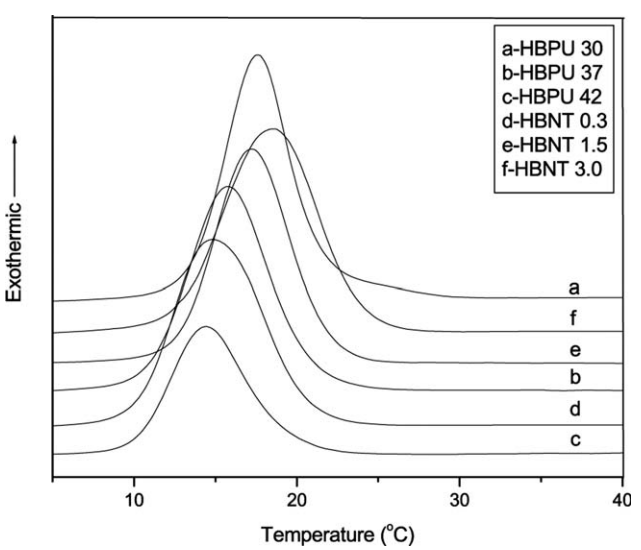


**Figure 6** DSC thermograms of pure HBPU and the MWNT/HBPU nanocomposites measured on cooling from the melt.

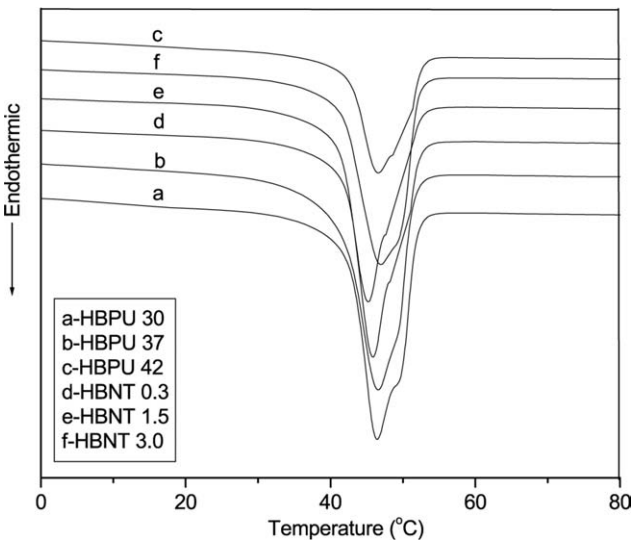


**Figure 7** DSC thermograms of pure HBPU and the MWNT/HBPU nanocomposites measured on second heating.

conformations were possible.[29] The structural perfection of hyperbranched polymers is usually characterized by the determination of their degree of branching (DB), which is determined here according to Frechet equation[30]: DB = $(D + T)/(D + T + L)$, where $D$, $T$, and $L$ refer to the number of dendritic, terminal, and linear units in the structure of the polymer, respectively. Experimentally, DB is generally calculated from NMR spectroscopy by a comparison of the integration of the peaks for the respective units in the hyperbranched polymer. The structure of the hyperbranched polymer is indeed a block construction of these three units. Therefore, DB was determined here by a comparison of the reacted and unreacted B functional groups, and the same were compared with the model compounds. With the help of $^1$H NMR measurement, it was found that the urethane (–O–CO–NH–) linkages derived from the –OH group of the $B_3$ monomers are sensitive to the number of B functional groups, and these can be used to assign DB. The peaks for the different units were assigned as discussed in the section on characterization. The value of DB for the polymer was found to be 0.57. This value indicates that the polymer exhibits near to highly branched structure rather than more linear structure (DB close to zero for linear, 0.5 for hyperbranched, and 1.0 for dendrimer; Scheme 1c). The synthesized polymers are soluble in highly polar organic solvents like *N*,*N*-dimethylformamide, *N*,*N*-dimethylacetamine, 1-methyl-2-pyrrolidinone, DMSO, etc., and they can be made soft and hard by varying with temperature. These results indicate that the polymers are thermoplastic in nature. X-ray diffraction patterns of HBPUs with different hard segments are determined. Pure HBPU showed diffraction peaks at $2\theta = 21.7°–22.1°$ and 24.1°–24.2° due to the presence of PCL crystals in the soft segments (Fig. 2). The molecular weight ($M_w$) and polydispersity index (PDI) of HBPU 37 obtained from GPC measurement were 4.4 $\times$ $10^4$ g/mol and 1.70, respectively. This confirms the synthesis of crystallizable *s*-triazine HBPU.

## MWNT dispersion into HBPU

The synthesized HBPUs were used to prepare well-dispersed MWNT nanocomposites. Dispersion and stability of MWNTs in the HBPU were observed using a solubility test in DMF solution after sonication. The HBPU/MWNT nanocomposites showed good dispersion in DMF solution even after 1 week. This may be due to the cage-like superstructure of HBPU, which can make MWNTs permeable into the polymer without any significant entanglements. Such an enhanced dispersion of MWNTs in the HBPU was also confirmed by SEM images of the cross-sectional fractured surface of the nanocomposites. Figure 3(a–c) shows the well-dispersed nature of individual MWNTs, where the bright dots indicate the broken ends of MWNTs. The bright dots increased with respect to MWNT content. Such an enhanced dispersion of MWNTs in the HBPU was also confirmed by TEM observation as shown in Figure 3(d–f). The presence of these individual MWNTs clearly indicates that the MWNTs were not broken or damaged, which contributes to the hyperbranched polymer-assisted dispersion. To investigate the surface properties, AFM studies have been carried out for HBPU/MWNT nanocomposites. Figure 4 represents the current images in 2D AFM measurements. The scale bar at *y*-axis means the current value

**TABLE II**
**Thermal and Shape Memory Properties of HBPU and Nanocomposites Used in This Study**

| Sample codes | Crystallization temperature (°C) | Heat of crystallization (J/g) | Melting temperature (°C) | Heat of fusion (J/g) | Crystallinity (%) | Shape retention (%) | Shape recovery (%) |
|---|---|---|---|---|---|---|---|
| HBPU 30 | 17.1 | 41.6 | 46.4 | 44.4 | 30.6 | 82 | 76 |
| HBPU 37 | 14.9 | 38.2 | 45.1 | 37.7 | 28.1 | 84 | 80 |
| HBPU 42 | 14.3 | 23.1 | 46.5 | 23.2 | 17.0 | 86 | 83 |
| HBNT 0.3 | 15.7 | 38.9 | 45.8 | 38.8 | 28.6 | 85 | 82 |
| HBNT 1.5 | 16.5 | 40.5 | 46.5 | 37.9 | 29.8 | 88 | 85 |
| HBNT 3.0 | 18.4 | 44.3 | 47.0 | 41.4 | 35.5 | 90 | 86 |

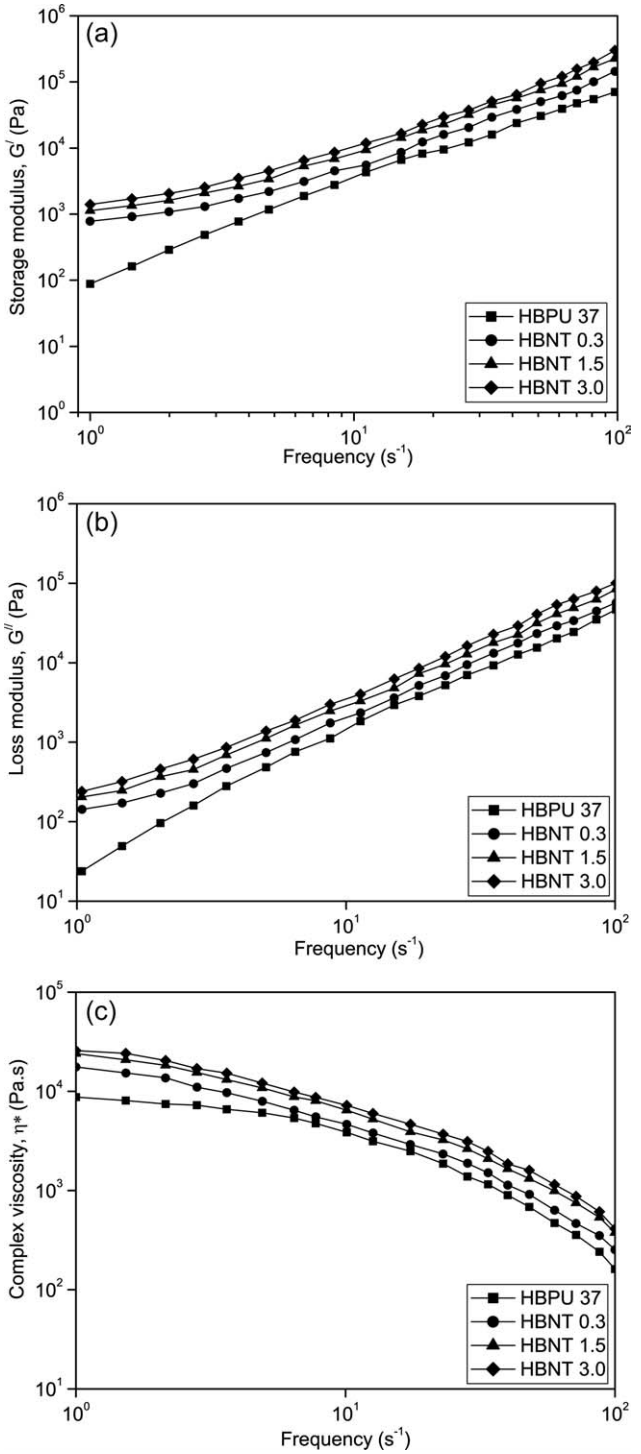


**Figure 8** Variation of storage modulus ($G'$; a), loss modulus ($G''$; b), and complex viscosity ($\eta^*$; c) of the HBPU and nanocomposites.

due to applied voltage in AFM current measurements, where the spots indicate presence of conducting materials, that is, CNTs. The 2D micrograph of the nanocomposite film reveals uniform distribution of MWNTs in the HBPU matrix without any agglomeration even at different weight percentage, which supports the importance of hyperbranched structure in terms of CNT dispersion.

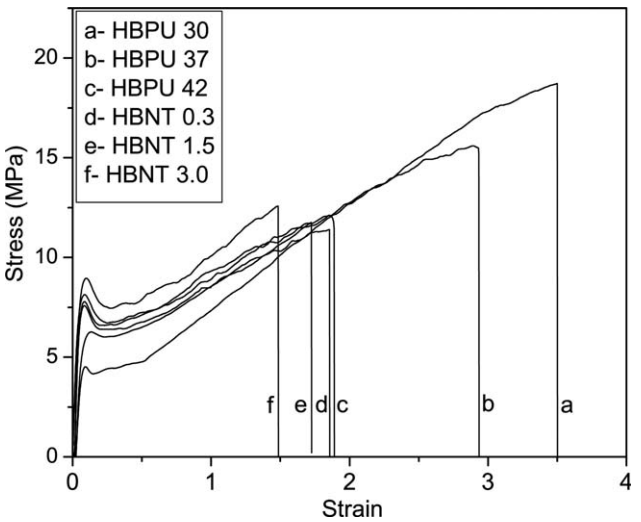


**Figure 9** Stress–strain curves of pure HBPU and MWNT/HBPU nanocomposites.

### Thermal and rheological properties of nanocomposites

The thermal nature of the HBPUs from TGA and DSC measurements is shown in Figures 5–7. The crystallization temperature ($T_c$), melting temperature ($T_m$), etc., are summarized in Table II. From Table II and Figure 6, it is seen that the crystallinity is significantly dependent on the hard segment and MWNT content. With an increase of hard segment, the crystallinity decreases due to less PCL crystals, whereas with an increase of MWNT content, the crystallinity increases due to nanotube-induced crystallization. For all the samples, the thermal degradation was observed (Fig. 5) in two steps because of the soft and hard segments in PU.[31] The overall good thermal stability may be due to the presence of triazine ring.[23–25] The degradation temperature of the nanocomposites shifted to significantly higher temperature compared to that of pristine HBPU. This is

**TABLE III**
**Mechanical Properties of HBPU and Nanocomposites**

| Sample code | Breaking stress (MPa) | Elongation at break (%) | Modulus (MPa) | Yield stress (MPa) | Yield strain (%) |
|---|---|---|---|---|---|
| HBPU 30 | 18.7 | 3.5 | 49.2 | 4.5 | 0.09 |
| HBPU 37 | 15.5 | 2.9 | 56.6 | 6.2 | 0.13 |
| HBPU 42 | 12.0 | 1.9 | 67.7 | 7.8 | 0.08 |
| HBNT 0.3 | 11.4 | 1.8 | 61.2 | 7.5 | 0.08 |
| HBNT 1.5 | 11.7 | 1.6 | 66.1 | 8.1 | 0.09 |
| HBNT 3.0 | 12.6 | 1.4 | 79.8 | 8.9 | 0.10 |

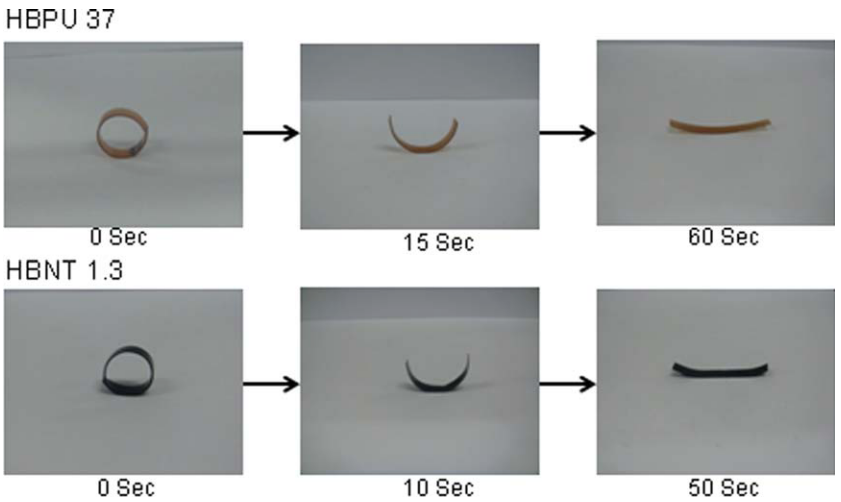


**Figure 10** Thermoresponsive shape recovery behaviors of pure HBPU and MWNT/HBPU nanocomposites. [Color figure can be viewed in the online issue, which is available at wileyonlinelibrary.com.]

attributed to the barrier properties of the nanotubes, which are responsible for enhancing the thermal stabilization of the nanocomposites.

The rheological properties of HBPU/MWNT nanocomposites are presented in Figure 8 for HBPU 37 and a range of MWNT weight fraction. It is noticeable that HBPU 37 exhibited a shear-thinning behavior with increasing frequency, indicating a pseudosolid nature of samples. The addition of MWNTs evidently increased the values of the storage modulus ($G'$), loss modulus ($G''$), and complex viscosity ($\eta^*$) in the entire frequency range. All the nanocomposites showed apparent plateau for both $G'$ and $G''$ at low frequencies [Fig. 8(a,b)]. The enhanced moduli also account for the increased mechanical properties of the nanocomposites, which were increased in the low-frequency region and decreased in the high-frequency region. Thus, oscillation-thinning behavior was observed for all the nanocomposites. The complex viscosity of HBPU/MWNT nanocomposites [Fig. 8(c)] decreased with increasing frequency, indicating a non-Newtonian behavior over the frequency range investigated. The smallest low-frequency slope of $G'$ versus frequency and the highest $G''$ at low frequencies for the nanocomposites indicate the homogeneous dispersion of the CNTs in the hyperbranched polymer matrix.[32]

### Mechanical and shape memory properties of nanocomposites

Figure 9 shows the stress–strain curves of the HBPU/MWNT nanocomposites. The mechanical properties of the nanocomposites depend on the hard segment content and the presence of MWNTs (Table III). The tensile strength and modulus increase with increasing the hard segment because of the physical crosslinking that depends on hydrogen bonding and dipole–dipole interaction. With increasing the hard segment content, the rigidity of the samples increases and thus it is difficult to allow high stretching. With an addition of MWNTs, the elongation-at-break of the nanocomposites decreases largely and the breaking stress decreases significantly compared to that of pure HBPU. However, the mechanical properties of the nanocomposites such as yield stress and modulus in the low-strain region up to 50% elongation show the large increase with an increase of MWNT content. It is because the well-dispersed MWNTs are increasingly networked among the HBPU chains, and so such structures may be effective in reinforcing stress of the samples, but may not allow the sample's elongation easily.

In addition to the mechanical properties, the MWNT dispersion may also affect other physical properties such as thermoresponsive shape memory properties of PCL-based PUs as shown in Table II. The PUs with different hard segment content (30–42 wt %) were synthesized to sustain their shape through inter- and intramolecular chain interactions such as hydrogen bonding, dipole–dipole interaction, and induced dipole interaction together with the physical crosslinking. The reason for using the specific molecular weight PCL (3000 g/mol) was furthermore to enhance the shape memory properties, where the soft segment is responsible for reversible phase transformation (Fig. 10). The *s*-triazine-based hyperbranched structure with aromatic ring may get advantages because of their large number of active functional group, which increase the interaction between the molecular chains. Shape recovery and shape retention were better for the ones with higher hard segment content (Table II). In particular, the HBNT 3.0 nanocomposites showed better shape recovery and shape retention, which are ascribed to the increased stored energy of the nanocomposite

due to the incorporation and good dispersion of MWNTs in the hyperbranched polymer matrix.

## CONCLUSIONS

*s*-Triazine-based HBPUs were synthesized successfully containing different hard segment and were used for preparing their MWNT-reinforced nanocomposites. The hyperbranched structure plays an effective role for enhancing the dispersion of pristine MWNTs into polymer matrix, and as a result, the HBPU–MWNT nanocomposites showed a steep increase in the mechanical properties and enhanced shape memory effect with an increase of hard segment and MWNT contents. For these inherent properties of HBPU, it may be useful in application as a MWNT dispersing agent for linear shape memory PU.

## References


1. Sreekumar, T. V.; Liu, T.; Min, B. G.; Guo, H.; Kumar, S.; Hauge, R. H.; Smalley, R. E. Adv Mater 2004, 16, 58.
2. Ajayan, P. M.; Schadler, L. S.; Giannaris, C.; Rubio, A. Adv Mater 2000, 12, 750.
3. Treacy, M. M.; Ebessen, T. W.; Gibson, J M. Nature 1996, 381, 678.
4. Ebbessen, T. W. Annu Rev Mater Sci 1994, 24, 235.
5. Thess, A.; Lee, R.; Nikolaev, P.; Dai, H.; Petit, P.; Robert, J.; Xu, C.; Lee, Y. H.; Kim, S. G.; Rinzler, A. G.; Colbert, D. T.; Scuseria, G. E.; Tomanek, D.; Fischer, J. E.; Smalley, R. E. Science 1996, 273, 483.
6. Gojny, F. H.; Nastalczyk, J.; Roslaniec, Z.; Schelte, K. Chem Phys Lett 2003, 370, 820.
7. Kumar, I.; Rana, S.; Rode, C. V.; Cho, J. W. J Nanosci Nanotechnol 2008, 8, 3351.
8. Hilding, J.; Grulke, E. A.; Zhang, Z. G.; Lockwood, F. J Dispersion Sci Technol 2003, 24, 1.
9. Youyong, X.; Gao, C.; Kong, H.; Yan, D.; Jin, J.-Z.; Watts, P. C. P. Macromolecules 2004, 37, 8846.
10. Yang, Y.; Xie, X.; Yang, Z.; Wang, X.; Cui, W.; Yang, J.; Yiu, W.-M. Macromolecules 2007, 40, 5858.
11. Jeon, I.-Y.; Lee, H.-J.; Choi, Y.-S.; Tan, L.-S.; Baek, J.-B. Macromolecules 2008, 41, 7423.
12. Gao, C.; Yan, D. Prog Polym Sci 2004, 29, 183.
13. Voit, B. J Polym Sci Part A: Polym Chem 2005, 43, 2679.
14. Voit, B. J Polym Sci Part A: Polym Chem 2000, 38, 2505.
15. Chen, H.; Yin, J. J Polym Sci Part A: Polym Chem 2002, 40, 3804.
16. John, W. C.; Bogart, V.; Gibson, E.; Copper, S. L. J Polym Sci Polym Phys Ed 1983, 21, 65.
17. Frontini, P. M.; Rink, M.; Pavan, A. J Appl Polym Sci 1993, 48, 2023.
18. Lendlein, A.; Langer, R. Science 2002, 296, 1673.
19. Lee, B. S.; Chun, B. C.; Chung, Y. C.; Sul, K. I.; Cho, J. W. Macromolecules 2001, 34, 6431.
20. Sahoo, N. G.; Jung, Y. C.; Yoo, H. J.; Cho, J. W. Macromol Chem Phys 2006, 207, 1773.
21. Sahoo, N. G.; Jung, Y. C.; Cho, J. W. Macromol Rapid Commun 2006, 27, 126.
22. Thostensona, E. T.; Renb, Z.; Chou, T.-W. Compos Sci Technol 2001, 61, 1899.
23. Mahapatra, S. S.; Karak, N. Mater Chem Phys 2008, 112, 1114.
24. Mahapatra, S. S.; Karak, N. Polym Degrad Stab 2007, 92, 947.
25. Wen, G.-A.; Xin, Y.; Zhu, X.-R.; Zeng, W.-J.; Zhu, R.; Feng, J.-C.; Cao, Y.; Zhao, L.; Wang, L.-H.; Wei, W.; Peng, B.; Huang, H. Polymer 2007, 48, 1824.
26. Ogoshi, T.; Saito, T.; Yamagishi, T.; Nakamoto, Y. Carbon 2009, 47, 117.
27. Star, A.; Stoddart, J. F. Macromolecules 2002, 35, 7516.
28. Chun, B. C.; Cha, S. H.; Chung, Y.-C.; Cho, J. W. J Appl Polym Sci 2002, 83, 27.
29. Silverstein, R. M.; Bassler, G. C.; Morril, T. C. Spectrometric Identification of Organic Compounds, 6th ed.; Wiley: New York, 1998.
30. Hawker, C. J.; Lee, R.; Frechet, J. M. J. J Am Chem Soc 1991, 113, 4583.
31. Chung, F. S.; Tsen, W. C.; Shu, Y. C. Polym Degrad Stab 2004, 84, 69.
32. Du, F.; Scogna, R. C.; Zhou, W.; Brand, S.; Fisher, J. E.; Winey, K. I. Macromolecules 2004, 37, 9048.